# Light tunneling in clouds

H. Moyses Nussenzveig

Solar radiation, traveling outside cloud water droplets, excites sharp resonances and surface waves by tunneling into the droplets. This effect contributes substantially to the total absorption (typically, of the order of 20%) and yields the major contribution to backscattering, producing the meteorological glory. Usual computational practices in atmospheric science misrepresent resonance contributions and cannot be relied on in the assessment of possible anomalies in cloud absorption. 

*OCIS codes:* 010.1300, 290.4020, 010.1310, 010.3640, 290.1090, 010.1290.

## 1. Introduction

Tunneling, a peculiar mode of wave propagation, is often regarded as a quantum effect, at the subatomic scale. However, it was discovered by Newton[1] as frustrated total reflection of light. Here I show that light tunneling plays an important role in the interaction of radiation with cloud water droplets. Rays incident outside the droplets excite resonances and surface waves by tunneling. Inadequate accounting for their contributions may have implications for the "anomalous cloud absorption mystery,"[2] a still unresolved and basic issue in climate studies.[3] Tunneling is the dominant effect in backscattering.[4] It produces the meteorological glory and is an essential ingredient of lidar cloud ranging. Common practices in Mie-scattering computations misrepresent resonance effects and must be amended to avoid substantial errors.

Hamilton's analogy between geometrical optics and classical mechanics, extended by Schrödinger to wave optics and quantum mechanics, yields a representation of monochromatic Mie scattering in terms of an effective square-potential-well picture.[4] For the $l$th partial wave in the Mie series, one must include the centrifugal term so that the effective radial potential becomes[4] a potential pocket surrounded by a (centrifugal) barrier. For droplet size parameter $x = ka \gg 1$ ($k$ = wave number, $a$ = droplet radius), van de Hulst's localization principle[5] associates the $l$th partial-wave angular momentum with an incident ray impact parameter $b_l = (l + \frac{1}{2})/k$.

We call below edge those partial-wave contributions for which $b_l < a$ and above edge those for which $b_l \geq a$. Below-edge incident rays hit the droplet, are refracted into it, and are multiply internally reflected and transmitted. Above-edge ones pass outside and, in geometrical optics, do not get scattered. In wave optics, they interact with the droplet by tunneling through the centrifugal barrier to the surface (evanescent wave coupling). Inside, they hit the surface beyond the critical angle, so that they would be totally reflected in geometrical optics, producing bound states of light (whispering-gallery modes). Tunneling to the outside, through the centrifugal barrier (curvature effect), converts bound states into resonances, with lifetimes exponentially sensitive to the depth below the barrier top. Rays close to the surface also give rise to surface waves that correspond to the diffracted rays of the geometric theory of diffraction.[6]

Mie resonances in highly transparent materials can attain large $Q$ factors, yielding numerous applications to nonlinear optics and cavity quantum electrodynamics.[7] They give rise to ripple fluctuations in Mie cross sections, a rapidly varying quasi-periodic pattern,[4,5] with quasi-period $\delta x$ approximately given by $\delta x \approx (\arctan \mu)/\mu$, where $\mu \equiv \sqrt{m^2 - 1}$ and $m$ is the real refractive index (for $m = 1.33$, one has $\delta x \approx 0.82$). Resonances can be parametrized in terms of their polarization, angular momentum $l$, and the analog $n$ of the principal quantum number. An efficient algorithm for highly accurate determination of all resonance locations and widths is available.[8] A

When this research was performed, the author was at NASA Goddard Space Flight Center, Greenbelt, Maryland 20771. His permanent address is Instituto de Fisica, Universidade Federal do Rio de Janeiro, Caixa Postal 68528, Rio de Janeiro 21945-970, Brazil. His e-mail address is moyses@if.ufrj.br.

Received 20 June 2002; revised manuscript received 28 October 2002.

0003-6935/03/091588-06$15.00/0

graphical representation of the optomechanical analogy is given in Appendix A.

### 2. Estimates of Mie Resonance Effects

A global estimate of the effect of Mie resonances on scattering is provided by their contribution to the mean density of states associated with the droplet, regarded as an open cavity. The ratio of the cavity density of states to that of the vacuum has been computed.[9,10] By applying complex angular momentum (CAM) techniques similar to those employed in obtaining average Mie efficiency factors,[4] I have evaluated size averages, which were taken over a size parameter range $\Delta x = \pi$, of the total Mie density of states and of that arising from only Mie resonances. Asymptotically, for $x \gg 1$, the ratio $R$ of the resonance contribution to the total mean density of states is given by[10] $R = (\mu/m)^3$. For $m = 1.33$, therefore, approximately 29% of the total mean density of states, for droplets much larger than the wavelength, arises from resonances, i.e., from above-edge rays. Each sharp resonance produces a Lorentzian peak with a unit area, which becomes a delta function in the limit of a cavity with impenetrable walls.

In absorption every resonance term is additive, so that $R$ already provides an order-of-magnitude estimate of the contribution from Mie resonances to water droplet absorption. Another estimate is obtained from the WKB approximation. We compare it with the geometrical-optics approximation to the absorption efficiency factor $Q_{\mathrm{abs}}$, given by[11]

$$Q_{\mathrm{abs,go}} = \frac{8}{3} m^2 (1 - R)\kappa x, \qquad (\kappa x \ll 1), \qquad (1)$$

where $N = m + i\kappa$ is the complex refractive index.

For $x \gg 1$ and $\kappa \ll 1$, the asymptotic WKB ratio of the average resonance contribution $\langle Q_{\mathrm{abs,res}} \rangle$ to the geometrical-optics result of Eq. (1) is found to be given by

$$\frac{\langle Q_{\mathrm{abs,res}} \rangle}{Q_{\mathrm{abs,go}}} = \frac{3}{4} \frac{\arctan \mu}{(m^3 - \mu^3)} \left[ \left( \frac{\mu}{\arctan \mu} \right)^2 - 1 \right]. \qquad (2)$$

The notation $\langle \cdots \rangle$ denotes an average over the quasi-period $\delta x$. The derivation of this estimate is outlined in Appendix B. For $m = 1.33$, the ratio of Eq. (2) is approximately 15.6%, again indicating that resonances yield a sizable contribution.

### 3. Results for Absorption

In atmospheric science, the recommended step size[12] in Mie computations is $\Delta x = 0.1$, and spectral band averages are commonly performed with values taken at the central band wavelengths alone.[13] Because resonances with widths much smaller than 0.1 proliferate in the size parameter ranges found in clouds, these practices lead to aliasing errors that contaminate radiative transfer calculations in comparisons between theoretical models and observations of cloud absorption.

Although computer power has increased by several orders of magnitude since the 0.1 resolution was recommended, so that localized brute-force approaches to include narrow-resonance contributions may be feasible, high-resolution Mie computations over broad spectral regions and size distributions are still impractical[14]; therefore computationally efficient parameterizations have been proposed.[14,15] However, these parameterizations do not apply to the rapidly varying regime associated with sharp resonances.

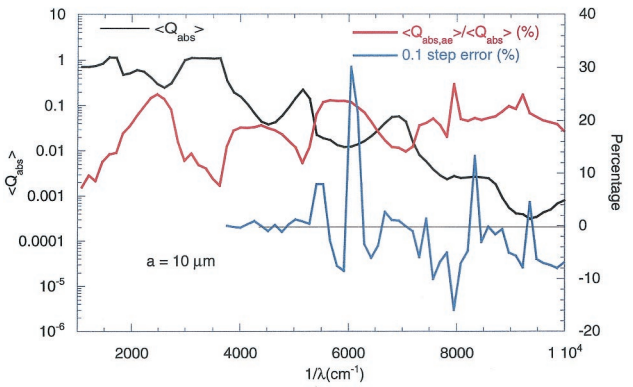


Fig. 1. Average spectral absorption efficiency of a 10-μm-radius water droplet in the near infrared. Black curve, Mie result (log scale); red curve, percentage that is due to tunneling (resonances); blue curve, percentage error when plotted at 0.1 steps in size parameter.

To get some idea of the contribution from resonances, and of the errors arising from a 0.1 step size, I considered a typical cloud water droplet, with $a = 10$ μm. I evaluated spectral averages $\langle Q_{\mathrm{abs}} \rangle$ over a quasi-period $\delta x = 0.8$, starting at $x = 7$, as well as the tunneling (above-edge) contribution $\langle Q_{\mathrm{abs,ae}} \rangle$, and compared the result, taking into account all resonances, with an evaluation at an 0.1 step size. The spectral range included, up to 10,000 $\mathrm{cm}^{-1}$, covers most of the domain where liquid water cloud absorption in a typical stratus cloud[16] occurs. The complex refractive index of water was taken from recent tabulations.[17,18]

The results are plotted in Fig. 1. They show that the tunneling contribution to absorption is of the order of 20% in this range, consistent with the above estimates. The 0.1 step errors take on some positive values (from occasional overestimation of resonance peak areas) that are due to the coarseness of the interval. In one case (in the visible spectrum) a 0.02 shift in sampled values of $x$ changes the error from −13% to +31%.

In the range above 5500 $\mathrm{cm}^{-1}$, where most of the cloud droplet absorption takes place,[16] the preponderant error is negative, originating from the missing resonance area. Sharper resonances tend to be entirely missed. Indeed, the likelihood of one hitting a sharp resonance at 0.1 steps is much smaller than that of one picking up the background [of the order of the geometrical-optics result of Eq. (1) plus the broadest resonance contribution], typically missing 5–10% of $\langle Q_{\mathrm{abs}} \rangle$.

An example of the aliasing effect around $x = 50$ is

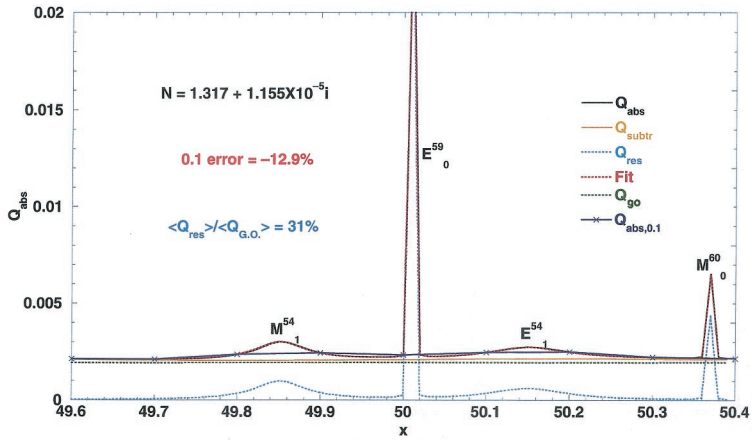


Fig. 2. Example of the aliasing effect of 0.1 step plotting for $N = 1.317 + 1.155 \times 10^{-5} i$. Solid black curve, Mie result; solid purple curve, 0.1 step result; dashed blue curve, pure resonance contribution; solid gold curve, nonresonant (background); dashed red curve, Lorentzian plus nonresonant (background) fit; dashed green curve, geometrical-optics approximation.

shown in Fig. 2. Within the illustrated quasi-period, there are four resonances, labeled by their polarization ($E$ or $M$), $l$ value (upper index), and $n$ (lower index). The two sharpest ones are entirely missed by the 0.1 step plot, resulting in an underevaluation of $\langle Q_{\mathrm{abs}} \rangle$ by 12.9%. If one subtracts from $Q_{\mathrm{abs}}$ the contribution $Q_{\mathrm{res}}$ from all four resonant Mie partial waves (also shown), one obtains the curve labeled $Q_{\mathrm{subtr}}$, which represents nonresonant (rippleless) Mie scattering. It does not differ much from the geometrical-optics approximation $Q_{\mathrm{go}}$ (Fig. 2).

The curve labeled fit in Fig. 2 is obtained when we add to the $Q_{\mathrm{subtr}}$ Lorentzian peak approximations to the resonance contributions, based on the uniform CAM approximation to the resonance locations and widths.[8] It is almost indistinguishable from the exact Mie curve. Thus one does not need to undertake time-consuming and costly plotting at fine steps to include the full resonance contribution: It suffices to plot the nonresonant Mie terms at 0.1 steps and to add the contributions from the resonances, treated as Lorentzians, with the uniform CAM approximation yielding the resonance parameters.

Results from the latest large-scale experiment on anomalous cloud absorption, Atmospheric Radiation Measurement Enhanced Shortwave Experiment II (ARESE II), are still unpublished. Preliminary data, presented at the Chapman Conference on Atmospheric Absorption of Solar Radiation (Estes Park, Colorado, August 2001), limit the anomaly to values below 10%, still subjected to instrumental and other uncertainties. The results shown in Fig. 1 are merely indicative: One must determine how they are affected by size averaging and by the effects of multiple scattering in radiative transfer. Going to larger size parameters, by inclusion of larger droplets or shorter wavelengths, should enhance resonance absorption. However, a definitive conclusion is that Mie calculations at 0.1 steps cannot be trusted when one is aiming at accuracies better than 10%. Thus the contribution from resonances must be included to arrive at reliable results concerning anomalous absorption.

## 4. Results for Backscattering

Light tunneling in clouds plays an even larger role in backscattering. This is relevant to the understanding of the beautiful natural phenomenon of the glory (Fig. 3), as well as to lidar cloud ranging.[20] In particular, the so-called lidar ratio, the ratio of backscattering to extinction, is the basis for lidar inversion.[21]

The backscattering gain $G(x)$, the ratio[5] of the Mie-backscattered intensity to that for an ideal isotropic scatterer, averaged over the quasi-period $\delta x = 0.8$ is plotted in Fig. 4 for a transparent droplet, with $N = 1.33007$, in the size parameter range 5–150. In this range, $\langle G \rangle_{\mathrm{Mie}}$ is of the order of 1.4, a value 40% higher than that for totally reflecting spheres and 14 times higher than the geometrical-optics result $\langle G \rangle_{\mathrm{go}}$. The below-edge contribution $\langle G \rangle_{\mathrm{be}}$ is the sum of many terms of near-peripheral origin. The tunneling term $\langle G \rangle_{\mathrm{ae}}$ is strongly dominant: Backscattering arises mainly from incident rays outside the droplets. However, there is also strong interference between this contribution and that from below-edge rays.

The curve labeled $\langle G \rangle_{\mathrm{CAM,nr}}$ is the lowest-order CAM approximation[4] to nonresonant backscattering gain. It is the sum of three gain terms: direct reflection, the tenth-order rainbow shadow, and the third Debye term.[4] The latter, which dominates $\langle G \rangle_{\mathrm{CAM,nr}}$ in this range, represents interference oscillations between the axial internally reflected ray and the van de Hulst surface-wave term[1,5] with a period

$$2\pi/\{\pi + 2 - 4[m - \mu + \arccos(1/m)]\},$$

which is $\approx$14 for $N = 1.33007$. A prior attempt[22] to compare CAM with $\langle G \rangle_{\mathrm{Mie}}$ misrepresented the van de Hulst term.

We can see from Fig. 4 that $\langle G \rangle_{\mathrm{CAM,nr}}$, which includes surface-wave tunneling effects, governs the qualitative behavior of $\langle G \rangle_{\mathrm{Mie}}$, with peaks and valleys


Fig. 3. Glory, photographed on clouds at the Haleakala crater in Maui. The estimated average droplet radius is near 9 μm (reproduced from Ref. 19 with permission by John C. Brandt, Institute for Astrophysics, University of New Mexico).

in the two curves closely matched. The large remaining contribution to $\langle G\rangle_{\mathrm{Mie}}$, which is also due to tunneling, arises from Mie resonances. The glory thus represents, in agreement with CAM theory,[4,23] a macroscopically visible tunneling effect.

## 5. Discussion and Conclusion

How good is the Mie model for actual cloud droplets? The presence of a central inclusion does not affect resonances, in view of their peripheral nature. Some types of insoluble off-center inclusion were found to attenuate the effect of the resonances.[24] However, if the inclusion is homogeneously distributed within the droplets (at least in an ensemble sense), it may increase the effective imaginary index and thereby strongly enhance the contribution from sharp resonances that would be smaller for pure water (Appendix B). A striking example is provided by carbonaceous soot clusters that form agglomerates within cloud droplets. It has recently been shown[25] that the absorption efficiency of weakly mixed soot under such conditions is enhanced by an average factor of approximately 25 over its value in vacuum for a broad range of size parameters. The reason for this increase is the enhancement by Mie resonances. Furthermore, the result was obtained by numerical integration, and it was changed from a previous estimate[26] of approximately 14 that had been based on the canonical 0.1 step. To obtain a reliable estimate for the enhancement factor, it was found necessary to decrease the step size below $10^{-3}$ for $100 < x < 200$ and below $10^{-5}$ for $x$ a few times larger.

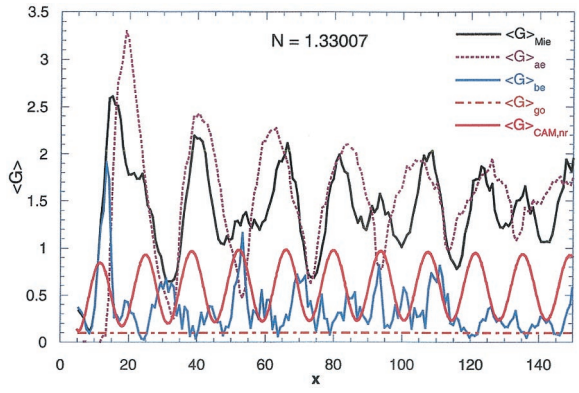


Fig. 4. Average backscattering gain factor of a transparent water droplet, with $N = 1.33007$, in the size parameter range 5–150. Shown are black curve, Mie result; purple dashed curve, above-edge; solid blue curve, below-edge; dashed–dotted red curve, geometrical-optics (go); solid red curve, CAM approximation to nonresonant (nr) contributions.

For a typical effective radius of 10 μm, the average droplet surface is highly spherical because of the strong dominance of surface tension.[27] Surface deformations, such as those produced by capillary waves, can lead to significant reductions of high $Q$ factors.[28] However, in the range of size parameters considered here, resonances with such $Q$ factors ($>10^6$) do not contribute appreciably. The average surface of a real droplet is not infinitely sharp, as in the Mie model. Its rounding off changes the top of the effective potential from a triangular to a rounded shape. This decreases near-barrier-top penetrability, sharpening the associated resonances and substantially enhancing their contribution. This effect

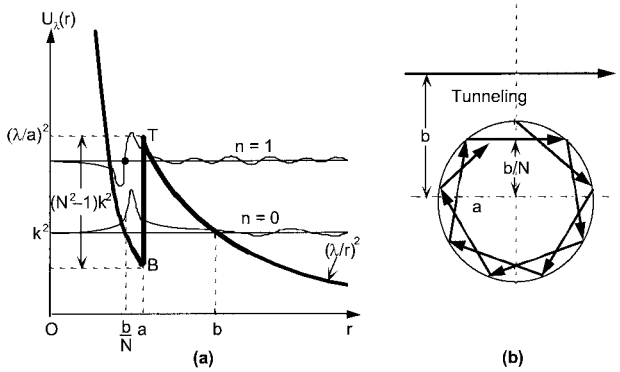


Fig. 5. (a) Effective radial potential $U_\lambda(r)$, $\lambda \equiv l + 1/2$, for a transparent sphere with $N > 1$ and angular momentum $l$. Narrow resonances arise in the domain between the top $T$ and the bottom $B$ of the potential pocket. Resonant wave functions with mode orders $n = 0, 1$ are sketched. (b) Associated ray picture according to the localization principle. The above-edge ray with impact parameter $b$ corresponds to the narrowest resonance, $n = 0$.

has been detected in scalar scattering.[29] The glory (Fig. 3), according to the above discussion, provides direct and visually stunning experimental evidence of the importance of resonances and light tunneling in clouds.

I have confined this discussion mainly to spherical water droplets. However, resonances and tunneling through (generalized) inertial barriers persist for small spheroidal deformations, although azimuthal degeneracy is broken.[30] The droplet aspect ratio varies with size, up to approximately 0.5 (oblate) before breakup.[31] Even for such large deformations, ripple fluctuations are still found in the efficiency factor for a spheroid as a function of size parameter.[32] Finally, above-edge tunneling effects (including surface waves and resonances) have also been detected and investigated, both theoretically and experimentally, for ice crystals in random and preferred orientations, as well as ice crystal aggregates in clouds,[33] by reference to equivalent ice sphere distributions with the same ratios of volume to average projected area. Thus it may be possible to extend the results of the present study to more general types of cloud.

### Appendix A: The Optomechanical Analogy

The effective radial potential[4] associated with a transparent droplet with real refractive index $N > 1$ and angular momentum $l$ is shown in Fig. 5(a). At resonant energies the radial wave function inside the potential pocket attains large intensities, localized near the droplet rim, corresponding to the ray picture of whispering-gallery modes represented in Fig. 5(b).

### Appendix B: WKB Estimate

Absorption represents an inelastic-scattering channel, so that the contribution to the absorption efficiency associated with a resonance pole $x_{l,n} - i\gamma_{l,n}$ in the elastic (transparent limit) partial-wave $S$ matrix for a given polarization is given by the Breit–Wigner formula[34]

$$Q_{\mathrm{abs},l,n}(x) = \frac{2l+1}{x^2}\,\frac{\gamma_{l,n}\gamma_{\mathrm{inel}}}{(x - x_{l,n})^2 + (\gamma_{l,n} + \gamma_{\mathrm{inel}})^2}, \quad \text{(B1)}$$

where $\gamma_{\mathrm{inel}} = \kappa x_{l,n}/m$ is the inelastic contribution to the total resonance width arising from material absorption.[8] Thus the total contribution from such a sharp resonance to $Q_{\mathrm{abs}}$ is the area under the Lorentzian peak:

$$\begin{aligned}\Delta Q_{\mathrm{abs},l,n} &= \pi(\text{peak value})(\text{total width}) \\ &= \frac{2\pi(2l+1)}{x_{l,n}^{\ 2}}\,\gamma_{\parallel,l,n}, \end{aligned} \quad \text{(B2)}$$

where

$$\frac{1}{\gamma_{\parallel,l,n}} \equiv \frac{1}{\gamma_{l,n}} + \frac{1}{\gamma_{\mathrm{inel}}}. \quad \text{(B3)}$$

From Eq. (B2), resonances with largest $\gamma_{\parallel,l,n}$ contribute most. Because the narrowest width dominates in Eq. (B3), we can base the estimate on only those resonances for which $\gamma_{l,n}$ is larger than or of the order of $\gamma_{\mathrm{inel}}$, ignoring the narrowest ones and taking $\gamma_{\parallel,l,n} \approx \gamma_{\mathrm{inel}}$. Thus, for the ratio of the resonant to the geometrical-optics contribution of Eq. (1), we find

$$\frac{\Delta Q_{\mathrm{abs},l,n}}{Q_{\mathrm{abs,go}}} \approx \frac{3\pi}{4}\,\frac{(2l+1)}{(m^3 - \mu^3)x_{l,n}^{\ 2}}. \quad \text{(B4)}$$

Summing over all resonances of both polarizations (a factor of 2), we obtain

$$\frac{\langle Q_{\mathrm{abs,res}}\rangle}{Q_{\mathrm{abs,go}}} \approx \frac{3\pi}{2}\,\frac{1}{(m^3 - \mu^3)\langle x^2\rangle}\sum_l (2l+1), \quad \text{(B5)}$$

where the sum extends over all resonances in a quasi-period.

The average spacing $\Delta l$ between terms in the above sum follows from previous WKB estimates[8]:

$$\Delta l \approx \frac{\partial l}{\partial x}\,\Delta x \approx \frac{\mu}{\arctan\,\mu}\,\frac{\pi}{\mu} = \frac{\pi}{\arctan\,\mu}. \quad \text{(B6)}$$

Thus

$$\begin{aligned}\sum_l (2l+1) &= \frac{(l_{\max})^2 - (l_{\min})^2}{2\Delta l} \\ &\approx \frac{\arctan\,\mu}{2\pi}\left[\left(\frac{\mu}{\arctan\,\mu}\right)^2 - 1\right]\langle x^2\rangle, \end{aligned} \quad \text{(B7)}$$

where WKB estimates[8] are used for the maximum and minimum values of $l$ in a quasi-period.

Substituting Eq. (B7) into Eq. (B5) we arrive at the result of Eq. (2).

It is a pleasure to thank Warren J. Wiscombe for valuable discussions and John C. Brandt for permission to reproduce Fig. 3. Useful suggestions by the

referees are gratefully acknowledged. This research was performed while the author held a National Research Council Research Associateship Award at NASA Goddard Space Flight Center. The author is also indebted to H. C. Bryant for Ref. 29.

## References


1. I. Newton, *Opticks*, 4th ed. (Royal Society, London, 1730), Book III, Part I, Query 29.
2. W. J. Wiscombe, "An absorbing mystery," Nature (London) **376,** 466–467 (1995), and references therein.
3. J. T. Houghton, Y. Ding, D. J. Griggs, M. Noguer, P. J. van der Linden, X. Dai, K. Maskell, and C. A. Johnson, eds., *Climate Change 2001: The Scientific Basis* (Cambridge U. Press, Cambridge, UK, 2001), p. 433.
4. H. M. Nussenzveig, *Diffraction Effects in Semiclassical Scattering* (Cambridge U. Press, Cambridge, UK, 1992).
5. H. C. van de Hulst, *Light Scattering by Small Particles* (Wiley, New York, 1957).
6. J. B. Keller, "Geometrical theory of diffraction," in *Calculus of Variations and its Applications*, L. M. Graves, ed. (McGraw-Hill, New York, 1958), pp. 27–52.
7. R. K. Chang and A. J. Campillo, eds., *Optical Processes in Microcavities* (World Scientific, Singapore, 1996).
8. L. G. Guimarães and H. M. Nussenzveig, "Uniform approximation to Mie resonances," J. Mod. Opt. **41,** 625–647 (1994).
9. S. C. Ching, H. M. Lai, and K. Young, "Dielectric microspheres as optical cavities: thermal spectrum and density of states," J. Opt. Soc. Am. B **4,** 1995–2003 (1987).
10. C. A. A. de Carvalho and H. M. Nussenzveig, "Time delay," Phys. Rep. **364,** 83–174 (2002).
11. C. F. Bohren and D. R. Huffman, *Absorption and Scattering of Light by Small Particles* (Wiley, New York, 1983).
12. J. V. Dave, "Effect of the coarseness of the integration increment on the calculation of the radiation scattered by polydispersed aerosols," Appl. Opt. **8,** 1161–1167 (1969).
13. A. Slingo and H. M. Schrecker, "On the shortwave radiative properties of stratiform water clouds," Q. J. R. Meteorol. Soc. **108,** 407–426 (1982).
14. D. L. Mitchell, "Parameterization of the Mie extinction and absorption coefficients for water clouds," J. Atmos. Sci. **57,** 1311–1326 (2000).
15. P. Chylek, P. Damiano, N. Kalyaniwalla, and E. P. Shettle, "Radiative properties of water clouds," Atmos. Res. **35,** 139–156 (1995).
16. R. Davies, W. L. Ridgway, and K.-E. Kim, "Spectral absorption of solar radiation in cloudy atmospheres: a 20 $cm^{-1}$ model," J. Atmos. Sci. **41,** 2126–2137 (1984).
17. D. M. Wieliczka, S. Weng, and M. R. Querry, "Wedge shaped cell for highly absorbent liquids: infrared optical constants of water," Appl. Opt. **28,** 1714–1719 (1989).
18. D. J. Segelstein, "The complex refractive index of water," M.S. thesis (Department of Physics, University of Missouri-Kansas City, Kansas City, Mo., 1981).
19. J. C. Brandt, "An unusual observation of the glory," Publ. Astron. Soc. Pac. **80,** 25–28 (1968).
20. R. M. Measures, *Laser Remote Sensing* (Wiley, New York, 1984).
21. J. D. Klett, "Lidar inversion with variable backscatter/extinction ratios," Appl. Opt. **24,** 1638–1643 (1985).
22. R. G. Pinnick, S. G. Jennings, P. Chylek, C. Ham, and W. T. Grandy, Jr., "Backscatter and extinction in water clouds," J. Geophys. Res. **88,** 6787–6796 (1983).
23. V. Khare and H. M. Nussenzveig, "Theory of the glory," Phys. Rev. Lett. **38,** 1279–1282 (1977).
24. D. Ngo and R. G. Pinnick, "Suppression of scattering resonances in inhomogeneous microdroplets," J. Opt. Soc. Am. A **11,** 1352–1359 (1994).
25. V. A. Markel, "The effects of averaging on the enhancement factor for absorption of light by carbon particles in microdroplets of water," J. Quant. Spectrosc. Radiat. Transfer **72,** 765–774 (2002).
26. V. A. Markel and V. M. Shalaev, "Absorption of light by soot particles in micro-droplets of water," J. Quant. Spectrosc. Radiat. Transfer **63,** 321–339 (1999).
27. A. Ashkin, "Applications of laser radiation pressure," Science **210,** 1081–1088 (1980).
28. J. P. Barton, "Effects of surface perturbations on the quality and focused-beam excitation of microsphere resonance," J. Opt. Soc. Am. A **16,** 1974–1980 (1999).
29. J. Wong, "Surface resonances in high-frequency scattering from a nearly-sharp three-dimensional well," M.S. thesis (Department of Physics and Astronomy, University of New Mexico, Albuquerque, N.M., 1968).
30. H. M. Lai, C. C. Lam, P. T. Leung, and K. Young, "Effect of perturbations on the widths of narrow morphology-dependent resonances in Mie scattering," J. Opt. Soc. Am. B **8,** 1962–1973 (1991).
31. H. Pruppacher and J. D. Klett, *Microphysics of Clouds and Precipitation* (Reidel, Dordrecht, The Netherlands, 1980), Fig. 10–15.
32. S. Asano, "Light scattering properties of spheroidal particles," Appl. Opt. **18,** 712–723 (1979).
33. A. J. Baran, P. N. Francis, S. Havemann, and P. Yang, "A study of the absorption and extinction properties of hexagonal ice columns and plates in random and preferred orientation, using exact *T*-matrix theory and aircraft observations of cirrus," J. Quant. Spectrosc. Radiat. Transfer **70,** 505–518 (2001).
34. L. D. Landau and E. M. Lifshitz, *Quantum Mechanics*, 3rd ed. (Butterworth-Heinemann, New York, 1997).